Materials Degradation in the Jovian Radiation Environment

Gennady Miloshevsky[1]
Purdue University, West Lafayette, Indiana, 47907

Jarvis A. Caffrey[2], Jonathan E. Jones[3], and Thomas F. Zoladz[4]
NASA Marshall Space Flight Center, Huntsville, Alabama, 35812

The radiation environment of Jupiter represents a significant hazard for Europa Lander deorbit stage components, and presents a significant potential mission risk. The radiolytic degradation of ammonium perchlorate (AP) oxidizer in solid propellants may affect its properties and performance. The Monte Carlo code MONSOL was used for modeling of laboratory experiments on the electron irradiation of propellant samples. An approach for flattening dose profiles along the depth of irradiated samples is proposed. Depth-dose distributions produced by Jovian electrons in multi-layer slabs of materials are calculated. It is found that the absorbed dose in a particular slab is significantly affected by backscattered electrons and photons from neighboring slabs. The dose and radiolytic decomposition of AP crystals are investigated and radiation-induced chemical yields and weight percent of radical products are reported.

I. Introduction

NASA's proposed Europa Lander mission is planned to launch in the late 2020s and would perform repeated gravitational maneuvers spanning multiple years before finally igniting a braking stage solid rocket motor to initiate entry, descent, and landing. Europa is embedded within the harsh radiation environment of the Jovian magnetosphere.[1] It is believed that much of the ionized plasma trapped in the Jovian belts is supplied by volcanic eruptions on Jupiter's moon Io. The radiation environment in the vicinity of Europa includes energetic electrons, protons, and heavier ions such as S^+, C^+, O^+. However, the bulk radiation damage to the spacecraft would be dominated by high fluxes of deeply penetrating electrons with the energy in excess of 100 MeV.[2] Europa Lander gravitational maneuvers will mostly occur in lower intensity regions around Jupiter at or beyond the orbit of Ganymede, and will experience the highest intensity of radiation in the final hours as it approaches Europa. A separate mission, Europa Clipper, will lay the foundation for Europa Lander and will be launched several years prior, accumulating an even greater total ionizing dose but with no requirement to engage a braking motor.

A typical solid propellant fuel used in rocket motors contains an oxidizer such as ammonium perchlorate (AP) (60-80%), a hydroxy terminated polybutadiene (HTPB) binder (10-15%), and aluminum powder (15-20%). Ammonium perchlorate (NH_4ClO_4) is an ionic crystal in which atoms are held together by ionic bonds. In the past decades, a large number of experimental and theoretical studies have been devoted to the investigation of thermal decomposition of AP crystals. The primary products of AP decomposition detected in many experiments are ammonia and perchloric acid. Therefore, it was proposed that the first step in AP decomposition is proton transfer.[3] The entire process involves several stages: 1) pair of NH_4^+ and ClO_4^- ions in AP lattice (see Fig. 1); 2) proton transfer from the cation NH_4^+ to the anion ClO_4^- in AP molecule; and 3) decomposition into ammonia NH_3 and perchloric acid $HClO_4$. The molecules of NH_3 and $HClO_4$ then react with the gas phase in AP crystal forming the products such as Cl_2, O_2, N_2, NO, N_2O, H_2O, etc. Concerning the mechanism of AP

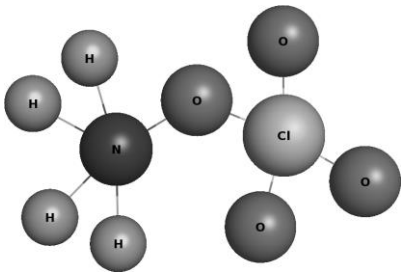

Figure 1. Ammonium perchlorate molecule NH_4ClO_4.

[1] Associate Professor, School of Nuclear Engineering, 400 Central Drive, Purdue University.
[2] Nuclear and Radiological Engineer, Propulsion Research (ER24), NASA MSFC.
[3] Technical Assistant, Solid Propulsion Devision (ER50), NASA MSFC.
[4] Branch Chief, Solid Separation and Maneuvering Systems Branch (ER52), NASA MSFC.

decomposition, it was established that the decomposition of single crystal orthorhombic AP at low temperatures (<513 K) is initiated by dislocation defects and occurs at mosaic crystal boundaries.[4] The decomposition further proceeds in a 3D manner consuming the boundary regions. AP crystals decompose only about 20 to 30% leaving a residue chemically identical with the original AP salt. The rate of thermal decomposition of AP was described by the Avrami-Erofeyev kinetic equation. The results of this earlier work are in contradiction with the recent study investigating the thermal decomposition of large single crystals of deuterated and non-deuterated AP at low-temperature.[5] It is found that at low temperature (250 °C) the decomposition proceeds inside the AP crystal with the desorption and transport of gaseous species from the bulk to the crystal's faces. The thermal decomposition stops when transformation of AP is about 30% with formation of the same porous products at lower (250 °C) and higher (350 °C) temperature. This limited decomposition of AP is in agreement with earlier predictions.[4] The slower decomposition of deuterated samples with 'snow' on the surface of AP crystals was observed.

The thermal decomposition of single crystal orthorhombic AP pre-irradiated by γ-rays was later investigated.[6] It was observed that the preliminary exposure of AP crystals to ionizing radiation shortens the time for thermal decomposition. The reaction rate constant of decomposition was found to be enhanced, accelerating the propagation of decomposition kinetics in the AP crystal. The change in the decomposition rate constant was attributed to the increase in the number of decomposition nuclei (presumably associated with dislocations) produced by the γ-radiation. The pure effect of γ-ray and X-ray irradiation on the decomposition of large AP crystals (5 x 3 x 3 cm) at room temperature in air and in the dark was experimentally studied.[7] The unirradiated AP crystals were water clear and free of inclusions and surface defects. Optical, transmission, and scanning electron microscopy were used to examine the irradiated AP crystals. At γ-ray doses between 10^3 and 10^5 rad, the AP crystals remained water clear and no radiation-induced defects were detected. At 1 Mrad irradiation, slightly opaque (milky) AP crystals were found with small, very flat pits on the *m* face similar to the pits formed during the early stages of thermal decomposition. At 5 Mrad γ-dose, the AP crystals became nearly opaque and milky white with circular pits and many tiny pits resolved by transmission microscopy on the *m* face. The γ-ray dose in 10 Mrad resulted in completely opaque AP crystals resembling white plastic. The formation of holes, channels, large bubbles, and cavities on some parts of the surface of AP was observed. The appreciable effect of X-rays on AP degradation was only observed at doses above 16 Mrad. The radiation-induced decomposition of AP was *found to be similar* in many respects to the thermal or chemically-induced decomposition. In both cases, there was an induction period during which the AP samples must receive the specific amount of heat or radiation dose before decomposition starts. The initial thermal, chemical or radiation effects caused the appearance of small pits that were aligned in some areas, but randomly distributed in other areas of the AP crystal. The characteristics of pits formed by thermal, chemical, or radiation treatment were quite similar on the first stage. They were roughly of the same size with density ~2 - 40 x 10^6 cm^{-2}, and aligned pits lie in the same crystal directions no matter how produced. On the second, or intermediate, decomposition stage, there was an extensive decomposition in all three treatment cases over the entire external crystal surface. At the last stage of decomposition, the separated blocks of undissolved crystals and "sponge-like" or coral structures containing rectangular voids were formed. However, there are the *specific effects induced by radiation* that were not observed during thermal and chemical treatment of AP. The high X-ray doses produced highly strained AP crystal with development of pronounced curvature, their fracture into blocks, and separation of blocks from the original crystal. The γ-ray induced decomposition occurred throughout the irradiated volume of the crystal, whereas the thermal and chemical decomposition started on the surface and penetrated inward. The sites of decomposition were localized inside the AP crystal where dislocations, slip planes, boundaries intersect. Therefore, the radiation-induced decomposition could not be simply related to the absorbed dose, since it occured only at dislocation-related sites, voids, cracks that are not randomly distributed in the AP crystal. Some mechanisms must exist for the transport of produced species from the location of each ionization event to decomposition sites.

The chemical reactions and compositional changes in AP induced by radiations can produce dramatically different microstructure and can have a profound influence on its properties. To date, very little research in radiation chemistry has been carried out in the field of the radiolysis of AP salts. The radiation-induced decomposition of AP into the various chemical fragments and their radiation-chemical yields (so called G values) were reported in the earlier experimental study.[8] G values represent the number of molecules of the product formed per 100 eV of absorbed ionizing energy. The study was performed over the dose range up to 120 Mrad using the source of ^{60}Co γ-rays. The radiolysis products of AP are found to be different than those for alkali metal perchlorates. The major products of AP radiolysis are chloride, chlorine, chlorate and hypochlorite. Their radiolytic yields in μmol/g are reported for different radiation doses. Chloride (Cl^-), chlorine ($C1_2$), and chlorate (ClO_3^-) have the largest G values. Chlorate was detected as the major product in the later study of γ-ray induced radiolysis of AP using IR spectro-photometry.[9] However, the other radiolytic products were not identified. The very recent study of the radiolytic decomposition of AP was conducted using various spectroscopy and spectrometry methods.[10] AP was exposed to

electrons at low temperature of 5.5 K. This very important work is a first experimental study of AP irradiated under cryogenic temperatures when primary chemical species created by radiation are immobile. Three different classes of molecules were detected: 1) nitrogen-based molecules NH_3, NH_2OH, N_2, and NO_2; 2) chlorine containing species ClO, ClO_2, and Cl_2O_3; and 3) oxygen molecules O_2. The first step of AP decomposition was confirmed to be deprotonation of NH_4^+. Ammonia (NH_3) may oxidize forming hydroxylamine (NH_2OH) or decay yielding molecular nitrogen (N_2). Perchlorate ions (ClO_4^-) can lose an oxygen yielding ClO_3^- and O. Molecular oxygen (O_2) is then formed via recombination of atomic oxygen (O). Chlorate (ClO_3^-) may further decompose into chlorite (ClO_2^-) and chlorine dioxide (ClO_2). However, G values for these species are not reported. These limited data are yet insufficient for the development of predictive models of radiation-induced degradation of AP at various temperatures.

The understanding of radiolytic decomposition mechanisms of AP are of great importance. It was established about 50 years ago in earlier experimental studies that the exposure of propellant to high energy radiation changes its composition and physical properties. However, the mechanism of the radiolytic decomposition of AP is not yet well understood. Therefore, the radiation effects on solid propellants during extended exposure to the Jovian radiation environment must be evaluated. The primary goal of this research is to develop theoretical models and computer codes as experimentally validated predictive tools for evaluations of AP degradation in the Jovian radiation environment. The main phases of this work should involve the evaluation of 1) deposited ionizing dose and atom displacement damage in the irradiated AP samples and multi-layer structures; 2) radiation-induced decomposition of AP due to breakage of chemical bonds with the creation of various fragments (radicals) of NH_3^+, ClO_4^-, HCl, H_2, O_2, H_2O, HNO, OH, ClO, Cl_2, N_2, NH_2, NO_2, etc.; and 3) long-time evolution of AP microstructure involving diffusion and chemical reactions between radicals, nucleation and growth of dislocations, defect clusters, precipitates, voids, and gas bubbles. The remainder of this report is organized as follows: In Section II, a description is provided of the MONSOL computer code used in this work for calculating the depth-dose profiles in materials. The modeling of laboratory irradiation experiments involving the mono-energetic electron beams is presented in Section III. Section IV contains a discussion of the results on the dose distribution in multi-layer materials due to an environmental source of electrons. The depth-dose distribution in a single AP crystal, radiolytic yield and weight percent of chemical radicals are reported in Section V. A summary is given in Section VI.

II. MONSOL Computer Code

The radiation dose deposited by high-energy particles in materials can be evaluated using the Monte Carlo (MC) transport approach. The MC method makes it possible to simulate random trajectories of electrons and photons as analogues to real particles using the theoretical cross sections of interaction processes. A three-dimensional MC model was developed and implemented in the MONSOL code[11] including all possible interactions of electrons and photons with materials. MONSOL was developed by the first author of this report, used in a number of practical applications, and has been well refined over the past years. The MONSOL code treats the coupled electron-photon transport.[12] The MC techniques implemented in MONSOL incorporate a mixed scattering model for the simulation of charged particle transport. Close collisions, with scattering angle and/or energy loss greater than predefined cutoff values are simulated in detail, by using analytical differential cross sections for the different interaction mechanisms and exact sampling methods. Distant collisions, with scattering angle or energy loss less than the corresponding cutoffs, are described by means of a multiple scattering theory. The interactions of photons with the medium are categorized primarily as the photoelectric effect, Compton scattering, and electron-positron pair production. The simulation of photon transport is straightforward since the mean number of interaction events in each history is fairly small. The MONSOL code is capable of carrying out numerical experiments on the effects of high-energy radiation (electrons, positrons, photons, ions and neutrons) on 3D configurations of solid-state composites. MONSOL was used recently in a project sponsored by National Nuclear Security Administration for investigating the correlation between different parameters (energy, angle, multiplicity, arrival time, etc.) of γ-ray and neutron radiation emitted from special nuclear materials.[13, 14] The details of the MONSOL code, benchmarks against results obtained from other MC codes, flowchart of the MC algorithm for tracing photons are described in these papers.

The recent validations of MONSOL results against the experimental data (calorimetric measurements performed at Sandia Laboratories)[15] on the energy deposition by MeV electrons into different materials are illustrated in Fig. 2. The specific goal was to validate the MONSOL code for materials such as C, Al, and hydrogen-rich compounds that are relevant to the present research. Fig. 2a and Fig. 2b show the energy deposition profiles in Al by electrons with 1.033 MeV for two incident angles of 0° and 60° to the surface normal, respectively. As the incident angle increases, the peak of absorbed energy is shifted toward the surface. The absorbed energy per unit mass of material is proportional to the absorbed dose. The maximum dose increases from ~3.2 MeV·cm^2/g for 0° to ~5 MeV·cm^2/g for 60°. This approach enables the major fraction of the absorbed dose to be localized near the surface of an irradiated

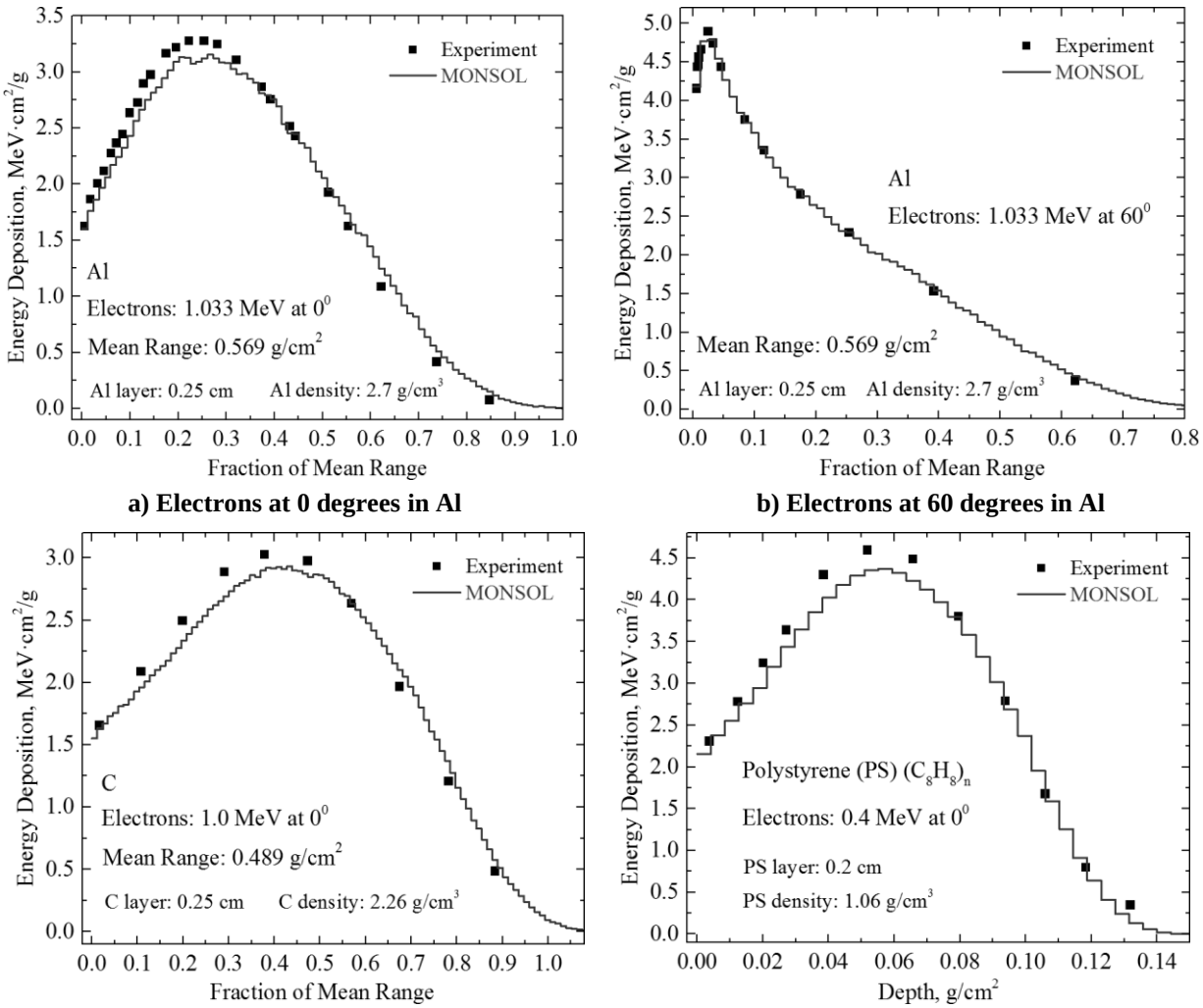

a) Electrons at 0 degrees in Al

b) Electrons at 60 degrees in Al

c) Electrons at 0 degrees in C

d) Electrons at 0 degrees in polystyrene

Figure 2. Profiles of energy deposition by monoenergetic electrons in different materials.

sample. The shapes of the theoretical histograms and the experimental curves are found in very good agreement, especially for 60°. The calculated location of the dose maximum and penetration depth of electrons agree closely with experimental measurements. The computational data are slightly lower in the vicinity of the peak for the 0° incidence angle. These differences can be attributed to experimental uncertainties or statistical errors in the MC technique. In Fig. 2c, the calculated dose distribution at normal incidence of electrons with 1 MeV for carbon is compared to the calorimetric measurements. The calculated and experimental peak positions of depth-dose distribution show very good agreement, although there appears to be a slight forward displacement of the calculated profile. It should be noted that the depth-dose distribution is affected by the material's density. The maximum absorbed dose is slightly higher and the dose peak occurs nearer to the surface for Al compared to that for C. In hydrogen-rich materials, there are more electrons per unit mass compared to high-*Z* elements. Therefore, the absorbed dose is higher (Fig. 2d) even for lower incident energy of electrons (0.4 MeV), since the energy deposition per unit length is proportional to the electron density. For polystyrene, the differences between the calculated and measured profile[16] of deposited energy are small (Fig. 2d). The peak position is nearly the same. The calculated value of absorbed dose at the peak of depth-dose distribution curve is slightly lower.

III. Modeling of Laboratory Irradiation Experiments

MONSOL modeling was performed for analysis of a HTPB hybrid propellant irradiation experiment using a mono-energetic electron beam at Marshall Space Flight Center. The irradiation experiment was performed as a pathfinder test plan in framework of the Europa DOS-Lander project. The experiment called for an available stock

of HTPB hybrid propellant samples to be exposed to approximately 6 Mrad of electron radiation. This level exceeds the expected dose to propellant anticipated in the Jovian environment by a factor of 5, as determined by separate analysis. The samples for testing were fabricated into slabs and dog-bones with thickness of one-fourth and one-half inch. The preference is to use samples of 1/2" thickness (1.27 cm) in order to conform with the JANNAF Class C dogbone standard. The samples were arranged on a plate within a 13" diameter circle and irradiated by mono-energetic 2 MeV electrons with electron fluence of 2.1×10^{14} e-/cm^2 and irradiation time of 520 minutes. The pre- and post-irradiated samples were then characterized to determine the effects of electron radiation on material properties such as modulus, hardness, electrical and thermal conductivity.

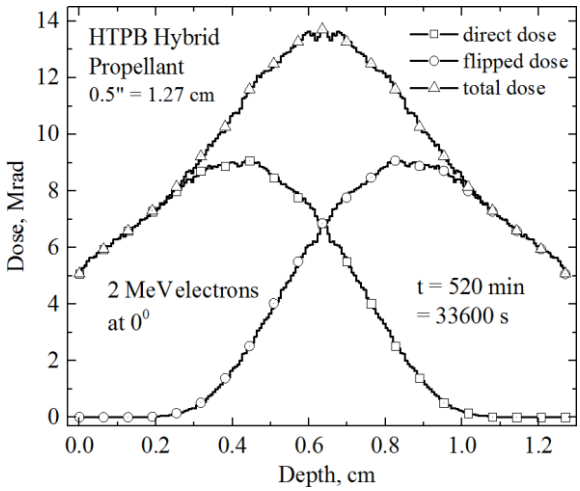

Figure 3. Depth-dose profiles in HTPB hybrid propellant irradiated by 2 MeV electrons.

There are two problems that should be solved in these irradiation experiments. First, the penetration depth of 2 MeV electrons in this material is about 1.1 cm, which is less than the thickness of 1/2" samples (Fig. 3, direct dose curve). This means that the backside of samples remains unirradiated. A way for resolving this issue is to flip the sample and perform an irradiation of the opposite side (Fig. 3, flipped dose curve). However, it is seen that the total accumulated dose (curve with open triangles) is much higher in the middle of the sample compared to that near the sample's faces. Second, it is highly desirable to produce a uniform (flat) dose distribution along the depth of sample. This is crucial for performing the post-irradiation tests of properties of samples. A standard approach to flatten the dose profile is to use successive electron beam irradiations with different energy and fluence. However, this requires multi-level and multi-time irradiations of both sides of samples, thus increasing time and cost of experiments. Furthermore, such a technique is only effective for a sample plate of all identical materials with identical thickness.

An alternative approach for flattening the total dose profile along the depth of an irradiated sample is proposed. The basic idea is to use a metallic plate placed in the front of the sample. Some dose in the rising portion of the depth-dose curve is then absorbed in a plate. The thickness of plate affects the shape of the remaining depth-dose profile in the sample. The more radiation dose that is absorbed in the plate, the higher is the dose near the surface of

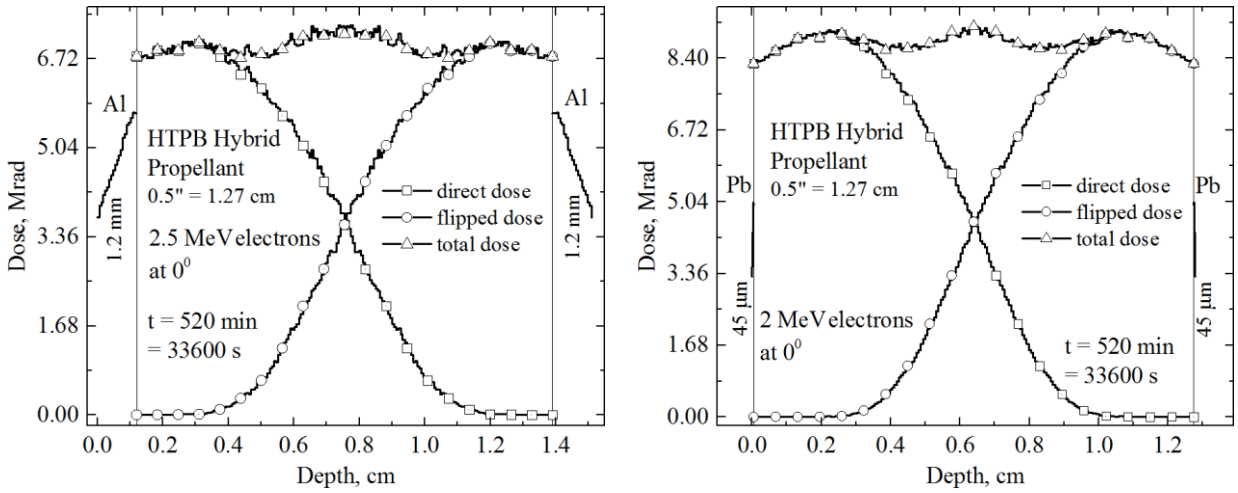

a) Dose flattening with Al plate **b) Dose flattening with Pb plate**

Figure 4. Dose-depth profiles in sample of HTPB hybrid propellant irradiated from front and back sides.

sample, up to a certain thickness. At a particular thickness of metallic plate, it is possible to achieve roughly a constant dose in the near-surface region of sample. This approach effectively eliminates the rising portion of the depth-dose curve and homogenizes the dose within a certain region near the surface of a sample. Among other benefits, this method also rules out the need to execute multiple irradiations of samples with different energies. For a thick sample, only two irradiations (one side and then the opposite side) are required. The flattened total depth-dose

profiles (curves with open triangles) in HTPB Hybrid Propellant with thickness 0.5" are illustrated in Fig. 4a and Fig. 4b for Al and Pb screens, respectively. It is seen that a sheet of Al with thickness ~1.2 mm is needed to achieve a constant dose (direct dose curve) near the surface of the sample. A much thinner film of Pb (~45 μm) can produce the same effect. However, the total absorbed dose in the propellant sample is increased ~25% when a high-*Z* metal is used. It should be noted that the absorbed dose distribution in a sample is affected by the incident energy of electron beam, thickness, and mass density of a sample. For example, the dose profile cannot be flattened by electrons with maximum energy of 2.5 MeV in a propellant of the same thickness as in Fig. 4 but higher mass density, since the electron range is shorter and the region in the center of sample might not be covered. There is a maximum thickness of material that can be treated using any of the aforementioned techniques, mainly driven by the maximum kinetic electron energy achieved by the accelerator. However, for samples within the viable range of thicknesses, the proposed approach should work well for homogenizing dose profiles in materials.

IV. Modeling of Depth-Dose Distribution in Materials due to Space Environment Electrons

A. Energy Spectrum of Jovian Electrons in Europa's Orbit

Materials used in spacecrafts are affected by energetic particles across a broad range of energy and particle species. The prediction of the radiation environment in the Jovian magnetosphere is based on the best available model to date such as the Galileo Interim Radiation Electron model v.2 (GIRE2).[17] This model relies on the data collected from the Galileo spacecraft which performed 35 orbits around Jupiter while measuring the radiation environment. The GIRE2 model is a useful tool for evaluating the electron environment for the future Europa Lander mission. Both the GIRE2 and the previous GIRE data map the particle energy spectra for electrons between tens of keV to more than one hundred of MeV, and also distribute said spectra across a spatial grid. Trajectory analysis through this grid then permits the approximation of the anticipated incident radiation environment on a given spacecraft. For the purpose of testing the implementation of a typical Jovian electron energy spectrum, some empirical models from available literature are used that describe the particle flux at Europa's orbit.[18] The modeled differential intensity of electrons (e^- per cm^2 s sr MeV) shown in Fig. 5, derived from these models, shows the degree of variation in both energy and intensity across many orders of magnitude. The electron flux (curve with open circles) is derived by the integration of differential intensity over the energy and solid angle. The energy flux (curve with open triangles) is obtained by averaging the energy of electrons using the differential intensity function. The legends at curves in Fig. 5 indicate the relevant units for a vertical axis on the left. The electron flux curve is used in the MC simulations to sample the energy of electrons impacting materials.

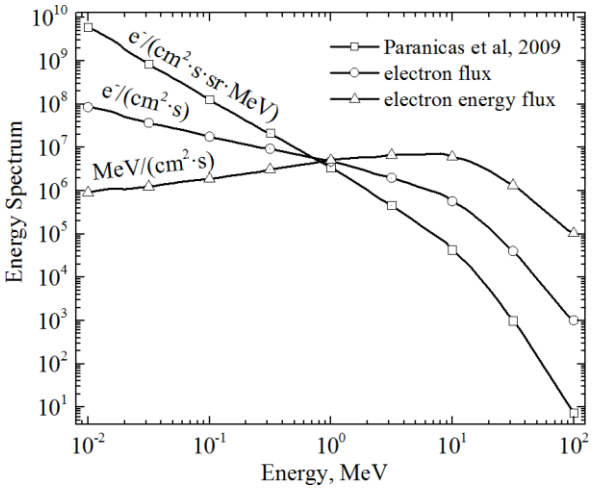

Figure 5. Energy spectrum of electrons determined near Europa's orbit.

B. Validation of MONSOL for Case of Environmental Spectrum of Electrons

Before describing the depth-dose profiles in multi-layer materials due to the effects of Jovian electrons, a benchmark is provided for MONSOL against the depth dose curves in Al for an experiment in literature that attempted to replicate the radiation environment at the standard geosynchronous orbit (GEO).[19] From that report, the total environment dose (curve with solid squares) and experiment dose (curve with solid circles) due to three beams of mono-energetic electrons of different energy and fluence are shown in Fig. 6. The largest drop in the depth-dose profile occurs in the near-surface layers (note log scale for dose and depth). It is seen that the depth-dose profile due to environment radiation can be approximated by using separate radiation sources of several beams of mono-energetic electrons and proper choice of fluences. The MONSOL code was set up to perform runs for each of three electron beams with energies and fluences indicated in Fig. 6. Two types of electron irradiation were modeled. First, a sample of Al was irradiated by each of three beams independently (sequential irradiation) (Fig. 6a). The three separate depth-dose profiles are illustrated. The agreement with portions of the total depth-dose profile (curve with solid squares) and the dose due to three beams (curve with solid circles) is quite good in almost all detail except for the case of 2 MeV electrons. The modeled penetration depth of electrons is slightly greater. Second, a sample of Al

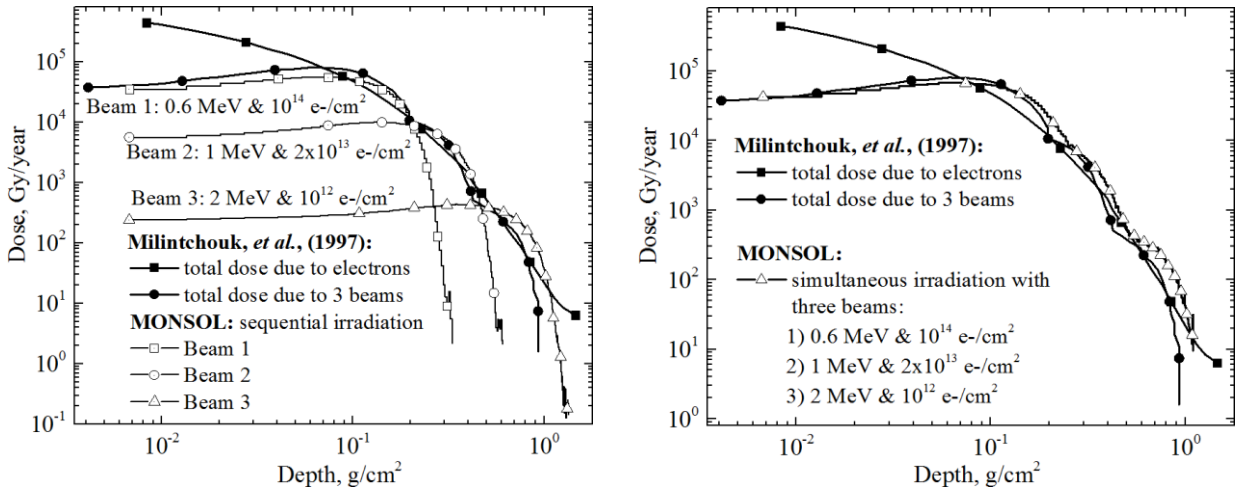

a) Sequential irradiation **b) Simultaneous irradiation**

Figure 6. Depth-dose profiles in Al for radiation environment at GEO orbit and for three beams of electrons of different energy and fluence.

was irradiated simultaneously (coupled irradiation) by three electron beams in a single MONSOL run. The resulting depth-dose profile is shown in Fig. 6b (curve with open triangles). Since the dose deposited in a material by different quasi-monoenergetic electron beams is additive, the sum of doses from three independent irradiations (Fig. 6a) should be equal to the total dose deposited by three simultaneous beams (Fig. 6b). The good agreement provides the confidence that the depth-dose profiles due to Jovian electrons would be predicted accurately.

C. Depth-Dose Distribution in Shielded Propellant at Europa's Orbit

In this subsection, we discuss the dose rate at Europa's orbit due to Jovian electrons absorbed in the multi-layer system composed of casing, insulator, liner, and propellant. The schematic is illustrated in Fig. 7. This system is irradiated by electrons in a wide range of energies from 10 keV to over 100 MeV. The electron energy spectrum

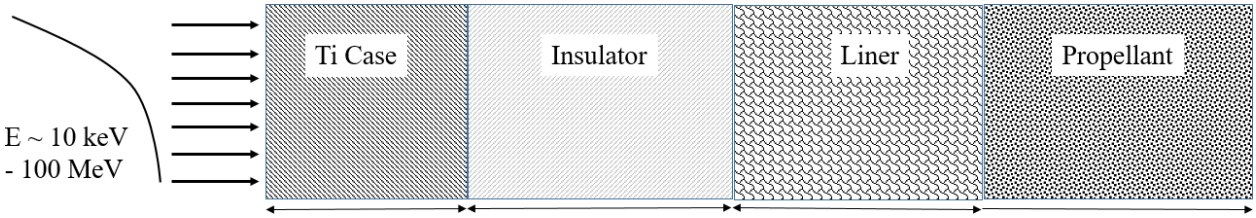

Figure 7. Schematic of multi-layer material slabs composed of Ti case, insulator, liner and propellant and irradiated by electrons with a wide spectrum of energies.

determined at the orbit of Europa[18] (Fig. 5) is used as a placeholder in our modeling of dose rate. This energy spectrum is representative of the approximate spectral shape, but does not accurately reflect the total fluence experienced by the spacecraft as it traverses the Jovian system. True incident fluences expected for the spacecraft must be calculated using the GIRE2 model that integrates the exposure using a spacecraft trajectory.[20] Since this method assumes a constant flux based upon the environment at Europa's orbit, it is possible to roughly anchor this analysis against a separate estimate of true incident dose rate and then assume a scaling factor in the form of an exposure time. The exposure time determined in this method does not represent actual exposure time of the spacecraft, as in reality it will pass through elliptical orbits with highly variable intensity. Still, it served its purpose in providing a convenient placeholder for incident fluence while developing the method for depth-dose analysis.

The normalized dose accumulated in slabs of different materials (Fig. 7) during one month of exposure to electrons at Europa's orbit is shown in Fig. 8. The slab of Ti receives the largest radiation dose in the near-surface region. This near surface dose would be even further enhanced due to a contribution of protons that are not considered in our modeling. Protons and heavy ions have a very short penetration depth on the order of tens of microns. The dose drops sharply along the depth of Ti case. The absorbed dose further decreases about two orders of

magnitude in a propellant layer. It is important to note that this assessment is based upon a representative energy spectrum of the radiation environment at Europa's orbit.

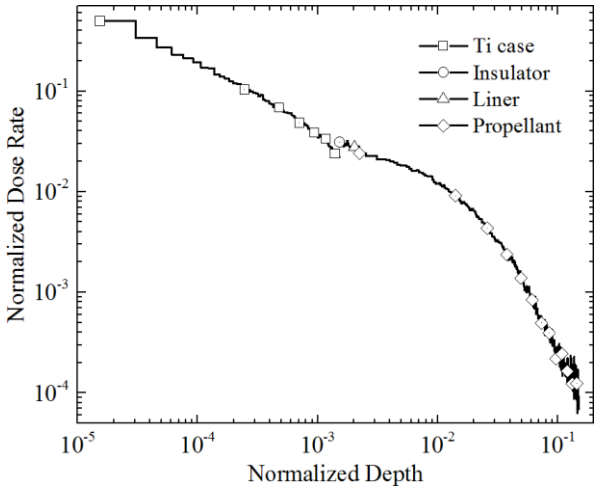

Figure 8. Depth-dose profile in the shielded propellant due to exposure to Jovian electrons at Europa's orbit during one month.

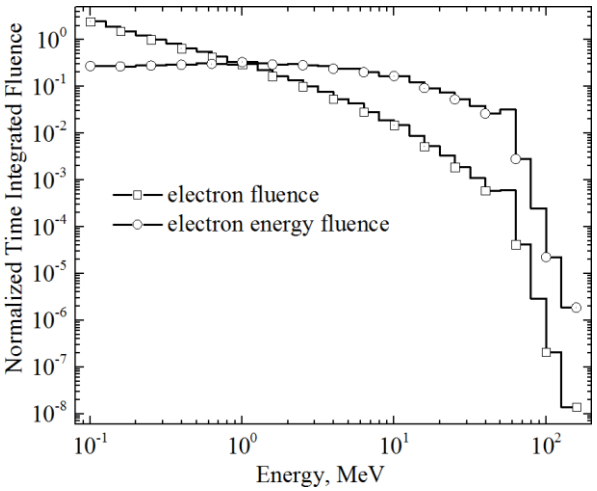

Figure 9. Total electron and energy fluence accumulated prior to Europa landing.

D. Depth-Dose Distribution in Propellant during Europa Lander Mission

The normilized time-integrated electron and energy flux giving the total electron and energy fluence through the entire Europa Lander mission are shown in Fig. 9. These data are derived from the GIRE2 model for a candidate spacecraft trajectory. This spectrum covering the energy range from 100 keV up to more than 150 MeV is used for evaluating the cumulative dose in an isolated Ti sheet and the multi-layer solid rocket motor system (Fig. 7).

The electron irradiation of a single layer of Ti was modeled. The depth-dose profile is shown in Fig. 10a. The depth-dose distribution in the four-layer system composed of Ti, insulator, liner, and propellant slabs and irradiated

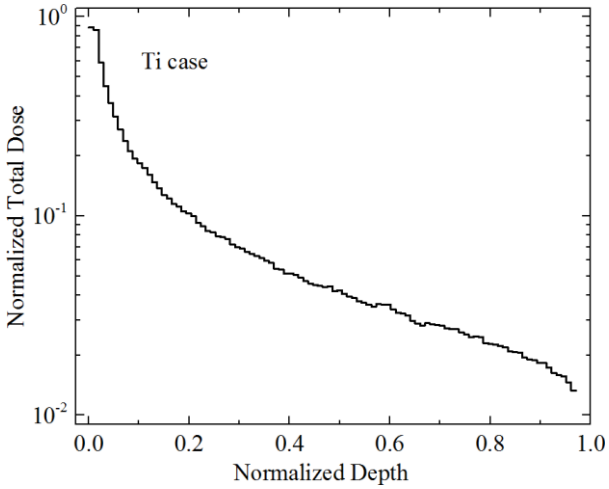

a) Single slab of Ti

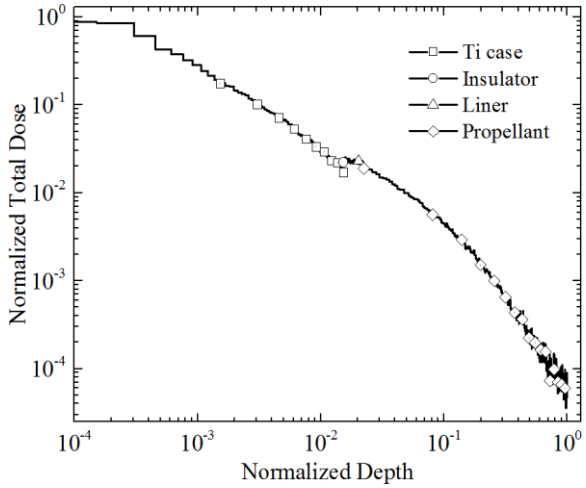

b) Slab of Ti followed by other slabs

Figure 10. Effect of truncation of multi-layer system on depth-dose profiles.

by Jovian electrons is shown in Fig. 10b. It is found that the value of dose behind Ti slab which is in direct contact with the rest of the multi-layer system (Fig. 10b) is about ~43% higher than the dose behind a single slab of Ti (Fig. 10a). The overdose is due to the contribution of neighboring slabs located behind a Ti sheet (Fig. 10b). We conclude that the depth-dose profile in a slab is affected when it is followed or preceded by other slabs of different materials. The effect is mainly due to the energy deposition by backscattered electrons and photons from neighboring layers of materials with very different properties.[21] Depth-dose distributions in multi-layer configurations depend strongly on

the atomic composition of particular materials as well as on their mass density. The build-up of energy deposition by radiation backscatter would be higher from the denser propellant. The percentage of the absorbed dose in the insulating and liner materials would be also considerably increased by the contribution from backscattering. It is noteworthy that accurate estimation of depth-dose distributions should be performed considering the irradiation of a multi-layer system, not just a single slab of material.

V. Radiolysis of AP by Energetic Electrons

A. Depth-Dose Distribution in AP Crystals Irradiated by 2 MeV Electrons

The depth-dose distributions in AP samples irradiated by energetic electrons serve as input data for radiolytic models of AP decomposition into radicals and chemical products. The depth-dose distributions produced by 2 MeV electrons in AP crystal were calculated using MONSOL, MCNP6, and EGSnrc computer codes and compared in Fig. 11. The dose is normalized per unit of fluence. The penetration depth of 2 MeV electrons in AP crystal is about ~0.6 cm. A good agreement is seen for the location of the peak energy deposition at ~0.18 cm predicted by MCNP6 and MONSOL. However, the height of dose peak yielded by MONSOL is reduced about ~8%, and as a consequence the rising portion of the depth-dose curve is shifted slightly deeper. The tails of depth-dose distributions obtained from both codes are in very good agreement. The height of peak dose predicted by EGSnrc is nearly the same as that yielded by MCNP6. The dose in the rising portion of the curve agrees well with that predicted by MONSOL. However, both the position of the dose peak and the falling portion of the energy deposition curve are shifted much deeper compared to the other two curves. This benchmark ensures that the depth-dose distribution produced by electrons in AP material is correctly calculated.

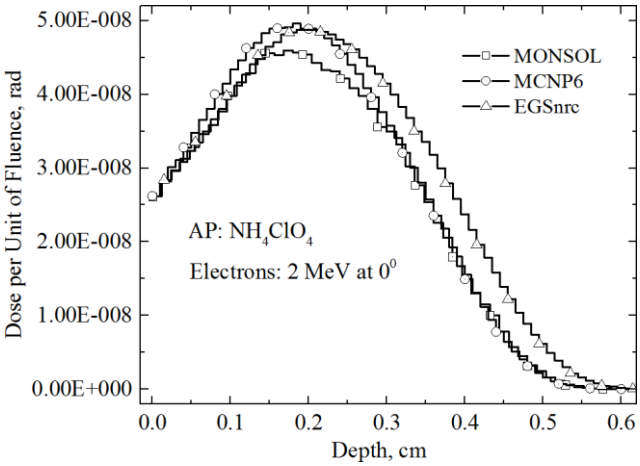

Figure 11. Depth-dose profiles for 2 MeV electrons in AP crystal at normal incidence calculated using three different codes.

B. Chemical Yields and Weight Percent of AP Products

Radiation yields of products are usually reported in terms of experimentally determined *G* values. Originally *G* value of product was defined as a number of product molecules produced per *100 eV* of absorbed energy. In the SI system the unit of *G* value is *mol/J*. The conversion factor between these two units is *1 mol/J = 9.648x10^6 molecules/100 eV*. The reported chemical products of the radiolysis of AP and approximate initial *G* values (molecules/100 eV) are as follows: Cl^- - 2.5; ClO_3^- - 1.3; $C1_2$ - 1.2; ClO^- - 0.45; $NO_3^- + NO_2^- < 0.05$; $ClO_2 < 0.02$; and $ClO_2^- < 0.02$.[8] These data were derived from the measurement of radiolytic yields of AP irradiated by a ^{60}Co source of γ-rays with absorbed doses higher than 8 Mrad.[22] The validity of these *G* values is less clear for lower doses of interest in our reseach. The initial yields of radiolysis products of AP were later summarized in a review paper.[23] The other data on *G* values were obtained in the experiments performed in the Soviet Union using 200 keV X-rays and 4.7 MeV protons. There is good agreement between the G values from different experiments. For example, the reported *G* values of Cl^- with highest yield are 2.1±0.1 (200 keV X-rays), 2.7 (4.7 MeV protons), and 2.5 (^{60}Co γ-rays). This provides some confidence in the accuracy of the reported *G* values. Unfortunately, the publications describing those original experiments and their dose levels are not available.[23]

The evaluation of radiolytic yield and weight percent of products in AP was performed for the Jovian electron environment with the time-integrated fluence (Fig. 9) accumulated during entire Europa Lander mission. The multi-layer system illustrated in Fig. 7 was used, but with propellant substituted with pure AP material. The calculated depth-dose profile in AP (not shown) was very similar to that shown in Fig. 10b for propellant. The chemical yield and weight percent of products in AP are shown in Fig. 12. The highest yield of Cl^- is ~4.8 μmol/g on the surface (Fig. 12a). The yield of Cl^-, ClO_3^-, $C1_2$ and ClO^- is prevailing in the near-surface region with its further decrease along the depth. Fluctations in the curves at the large depth arise from limited MC statistics. The yield of $NO_3^- + NO_2^-$, ClO_2 and ClO_2^- is insignificant, since their *G* values are small. The yield of ClO_2 (shown) and ClO_2^- (not shown) is the same because they share equal *G* values. The weight percent curves of products as a function of the depth shown in Fig. 12b resemble those of the chemical yield. Nevertheless, there is one distinction. In contrast to

the chemical yield, the weight percent of ClO_3^- on the surface is highest, ~0.021. This is because the molar mass of ClO_3^- is greater than the molar masses of Cl^- and $C1_2$. Overall, it can be concluded that the content of products in AP expected during spacecraft approach to Europa is very low.

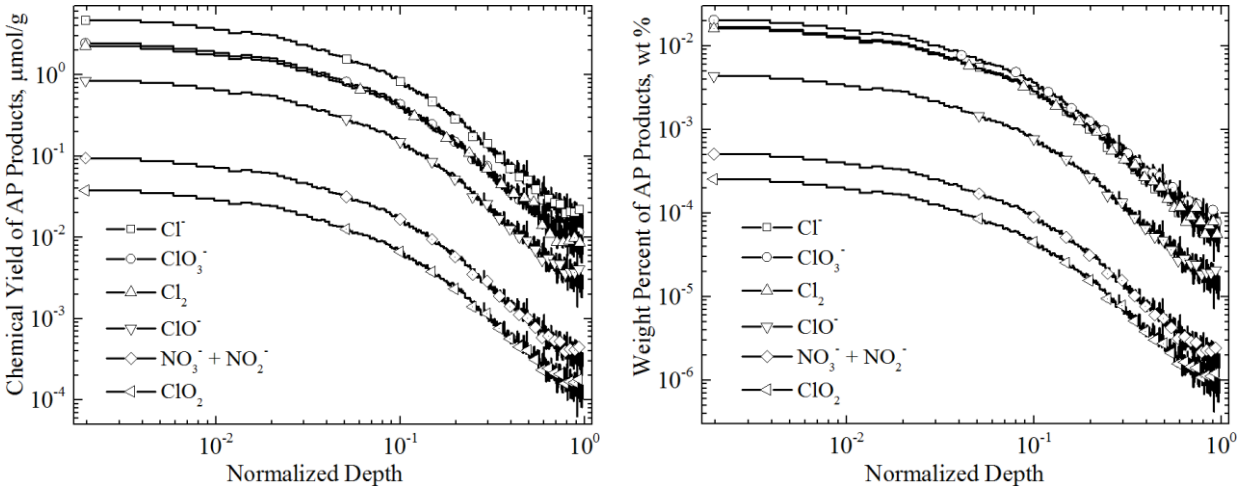

a) Chemical yield **b) Weight percent**

Figure 12. Chemical yield and weight percent of radiolytic products in AP irradiated by Jovian electrons during Europa Lander mission.

C. Future Developments

Further experimental and computational research is needed on the development of models for realistic predictions of radiation-induced decomposition of AP crystals. First, there is a lack of parameters needed in computational models such as 1) threshold energies for displacement of AP atoms from their lattice sites; 2) values of energy required to break bonds for N, Cl, O, and H atoms in AP; 3) rate constants describing chemical reactions between radiation-produced reactive radicals; 4) diffusion coefficients describing diffusion of chemically inert species in AP; and 5) rate constants for reaction of chemically stable species with dislocations, voids, bubbles, grain boundaries, and precipitates developed in AP crystals. Both experimental measurements and classical or quantum Molecular Dynamics simulations can be used as a source of these parametric data. Second, the algorithms and models have to be developed and implemented for 1) production of chemical radicals: this model describing the chemical yield of AP products is already implemented (Subsection B), but it has to be extended to include other possible species to be identified in future research; 2) prediction of chemical reactions between reactive radicals with formation of chemically inert products; 3) prediction of diffusion of produced chemically stable species in AP; 4) prediction of nucleation and growth of dislocations, voids, bubbles, etc.; and 5) prediction of reactions of stable species with dislocations, grain boundaries, voids, and bubbles. The depth-dose distributions in AP crystals calculated using MONSOL and described in this report will be used as a source term in many of these models.

VI. Conclusion

The depth-dose distributions produced by the impact of mono-energetic as well as space environment electrons on single-layer and multi-layer materials are studied using the MONSOL code. An approach using a forefront metallic plate for homogenizing the dose profile along the sample's depth in laboratory irradiation experiments is proposed. It is found that the dose absorbed in a particular slab of material sandwiched between other slabs is considerably increased due to the energy deposition by backscattered electrons and photons from neighboring slabs. It is recommended that dose evaluations to be performed considering the irradiation of a full multi-layer system rather than isolated slabs of material. It is found that the weight percent of chemical products accumulated in AP during Europa Lander mission is low. Future research should incorporate the calculated depth-dose profiles in the models describing chemical reactions between AP products and their diffusion, thus predicting degradation of AP.

Acknowledgments

G. Miloshevsky thanks the NASA MSFC Summer Faculty Fellow Program managers and staff for supporting this research that allowed him the opportunity to closely collaborate with MSFC engineers and scientists.

References

[1]Kivelson, M. G., Khurana, K. K., and Volwerk, M. "Europa's interaction with the Jovian magnetosphere." Univ. of Ariz. Press, Tucson, Ariz., 2009, pp. 545-570.

[2]Paranicas, C., Mauk, B. H., Khurana, K., Jun, I., Garrett, H., Krupp, N., and Roussos, E., "Europa's near-surface radiation environment," *Geophysical Research Letters*, Vol. 34, No. 15, 2007, p. L15103.

[3]Boldyrev, V. V., "Thermal decomposition of ammonium perchlorate," *Thermochimica Acta*, Vol. 443, No. 1, 2006, pp. 1-36.

[4]Galwey, A. K., and Jacobs, P. W. M., "The thermal decomposition of ammonium perchlorate at low temperatures," *Proceedings of the Royal Society of London, Series A*, Vol. 455, No. 1279, 1960, p. A254.

[5]Majda, D., Korobov, A., Filek, U., Sulikowski, B., Midgley, P., Vowles, D., and Klinowski, J., "Low-temperature thermal decomposition of large single crystals of ammonium perchlorate," *Chemical Physics Letters*, Vol. 454, No. 4, 2008, pp. 233-236.

[6]Herley, P. J., and Levy, P. W., "Thermal Decomposition of Irradiated Orthorhombic Ammonium Perchlorate," *Nature*, Vol. 211, No. 5055, 1966, pp. 1287-1288.

[7]Herley, P. J., and Levy, P. W. "Microscopic observations of X-ray and gamma-ray induced decomposition of ammonium perchlorate crystals," *Washington Proc. of the Natl. Symp. on Nat. and Manmade Radiation in Space*. NASA, 1972, pp. 584-594.

[8]Odian, G., Acker, T., and Pletzke, T., "γ-Radiolysis of Ammonium Perchlorate," *The Journal of Physical Chemistry*, Vol. 69, No. 7, 1965, pp. 2477-2479.

[9]Dedgaonkar, V. G., and Sarwade, D. B., "Studies on gamma radiolysis of microcrystalline ammonium perchlorate," *Journal of Radioanalytical and Nuclear Chemistry*, Vol. 199, No. 3, 1995, pp. 191-196.

[10]Gobi, S., Bergantini, A., Turner, A. M., and Kaiser, R. I., "Electron Radiolysis of Ammonium Perchlorate: A Reflectron Time-of-Flight Mass Spectrometric Study," *The Journal of Physical Chemistry A*, Vol. 121, No. 20, 2017, pp. 3879-3890.

[11]Miloshevsky, G. V. "The MONSOL code: Technical description." Luikov Institute of Heat and Mass Transfer, Minsk, Belarus, 2000.

[12]Leroy, C., and Rancoita, P. G. *Principles of Radiation Interaction in Matter and Detection*: World Scientific, Singapore, 2004.

[13]Miloshevsky, G., and Hassanein, A., "Energy–angle correlation of neutrons and gamma-rays emitted from an HEU source," *Nuclear Instruments and Methods in Physics Research Section A: Accelerators, Spectrometers, Detectors and Associated Equipment*, Vol. 749, 2014, pp. 47-56.

[14]Miloshevsky, G., and Hassanein, A., "Multiplicity correlation between neutrons and gamma-rays emitted from SNM and non-SNM sources," *Nuclear Instruments and Methods in Physics Research Section B: Beam Interactions with Materials and Atoms*, Vol. 342, 2015, pp. 277-285.

[15]Lockwood, J. G., Ruggles, E. L., Miller, H. G., and Halbleib, A. J. "Calorimetric measurement of electron energy deposition in extended media - Theory vs experiment." Sandia National Laboratories report SAND79-0414, Albuquerque, New Mexico, 1987.

[16]McLaughlin, W. L., and Hussmann, E. K. "The measurement of electron and gamma-ray dose distributions in various media," *Proc. of Symp. on Utilization of Large Radiation Sources and Accelerators in Industrial Processing*. IAEA STI/PUB/236, International Atomic Energy Agency, Vienna Munich, 1969.

[17]Garrett, H. B., Kokorowski, M., Jun, I., and Evans, R. W. "Galileo Interim Radiation Electron Model Update - 2012." JPL Publication 12-9, Jet Propulsion Laboratory, California Institute of Technology, Pasadena, CA, 2012.

[18]Paranicas, C., Cooper, J. F., Garrett, H. B., Johnson, R. E., and Sturner, S. J., "Europa's radiation environment and its effects on the surface," *in Europa, The University of Arizona space science series, edited by R. T. Pappalardo, W. B. McKinnon, K. K. Khurana, and R. Dotson (University of Arizona Press, Tucson)* 2009, pp. 529-544.

[19]Milintchouk, A., Van Eesbeek, M., Holmes-Siedle, A., and Levadou, F. "Degradation of materials under the action of soft X-ray radiation from solar flares," *Proc. 7th Int. Symposium on Materials in Space Environment*. Toulouse, France, 1997, pp. 87-96.

[20]de Soria-Santacruz Pich, M., Garrett, H. B., Evans, R. W., Jun, I., Kim, W., and Paranicas, C. "The GIRE2 model and its application to the Europa mission," *2016 IEEE Aerospace Conference*. 2016, pp. 1-7.

[21]Tabata, T., and Ito, R., "An Algorithm for Electron Depth-Dose Distributions in Multilayer Slab Absorbers," *Japanese Journal of Applied Physics*, Vol. 20, No. 1, 1981, p. 249.

[22]Odian, G., Acker, L., Pletzke, T., Henley, E., and McAlevy III, R. F. "Radiation Induced Solid Propellant Decomposition." Tech. Documentary Report on Contract AF 49 (638)-1125, Radiation Applications Inc., 1964.

[23]Zakharov, Y. A., and Nevostruev, V. A., "Radiolysis of Solid Inorganic Salts with Oxygen-containing Anions," *Russian Chemical Reviews*, Vol. 37, No. 1, 1968, p. 61.